Test of a RICH prototype at the CERN T9 beam line

June 22, 2013

Contents

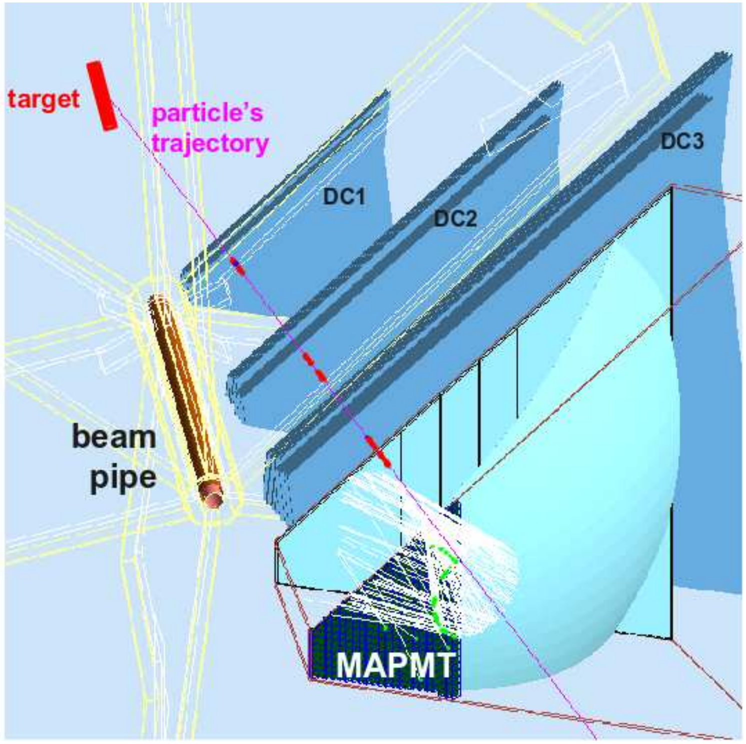

Figure 1: Layout of one sector of the RICH detector, placed just after the third region of Drift Chambers (DC3).

1 The CLAS12 RICH

Since the RICH detector must fit into the original CLAS carriage there are several constraints imposed upon its design. Six radial sectors are required, each with projective geometry, limited gap depth of 1.2m and 6 m^2 entrance windows. There is also a strict low material budget to minimise in the TOF detectors positioned behind the RICH. Simulation studies favour a hybrid imaging RICH design incorporating aerogel radiators, visible light photon detectors, and a focussing mirror system. The focussing mirror system (see Fig. 1) will be used to reduce the detection area instrumented by photon detectors to about 1 m^2 per sector, minimising costs and influence on the TOF system. For forward scattered particles ($\theta < 12o$) with momenta p = 3 - 8 GeV/c a proximity imaging method will be used, where the Cherenkov cone is imaged directly. For larger incident particle angles of $12^o < \theta < 35^o$ and intermediate momenta of p = 3 - 6 GeV/c the Cherenkov light will be focussed by an elliptical mirror, followed by two further passes through the radiator material and a reflection from planar mirrors before detection. The Cherenkov light will be produced from a thicker amount of aerogel material than it will be reflected through, to compensate yield losses whilst obtaining a focalised ring. For momenta below 3 GeV/c the TOF system will provide the pion/kaon separation for polar angles up to 40^o.

This RICH configuration is challenging in two major points: (i) the pion rejection factor necessary to correctly identify kaons, and (ii) the number of photoelectrons surviving the multiple pass through the aerogel. Some aspects of these questions have been addressed in laboratory tests, as for example measurements of the optical properties of the aerogel or the single photon response of the MAPMTs. However, a necessary step of this project is the validation of the proposed RICH geometry in conditions as close as possible to the real measurements. For this, a campaign of test beam has been undertaken in 2011 and 2012, using hadron as well as electron beams and prototypes of increasing complexity.

A first, preliminary, test has been performed in july 2011 at the T9 beam line of CERN using a simplified prototype, made by an aerogel radiator of variable thickess and refractive index, about 30 cm of gap and eight MAPMTs H8500. This first test showed that the chosen MAPMTs were actually capable to detect single photons also in the real experimental conditions and that the photon yield was sufficiently high to encourage further studies.

In 2012, a test has been performed at the Frascati Beam Test Facility (BTF) in order to setup the necessary acquisition system.

Finally, two new test beams have been performed using a large scale prototype specifically designed to provide the proof-of-principle of the detector. These tests have been done at the T9 test beam of CERN. Results of these tests will be extensively discussed in the next sections.

2 Prototype construction

In the real detector, the particles are revealed basically in two different conditions:

- for forward particles, the Cherenkov photons are directly detected by the MAPMTs;
- for large angle particles, the photons are detected after two reflections and a double pass through the aerogel radiator.

The third condition, in which part of the photons are detected directly and part after reflections, can be estrapolated from the two previous ones. Therefore, the design of the setup must be flexible enough to allow the necessary measurements in the two main conditions.

The RICH prototype has been build at LNF inside a large (approximately $1.6 \times 1.8 \times 1.6$ m^3) light-tight box, with internal modular supports holding the various components, that may be inserted or removed.

The Fig. 2 shows the schematic view, the project design and the realization of the prototype for the direct light measurements. The Cherenkov light is produced on the aerogel radiator, propagate for 1m inside the box and is then detected by an array of 28 MAPMTs, alternated of the type H8500C with normal glass and H8500C-03 with UV glass. The aerogel support can host tiles of approximately 58×58 mm^2 and of different thickness. The MAPMTs are mounted on a circular support and can be radially moved so to intercept the Cerenkov ring produced with different opening angles depending on the refractive index. The ring coverage varyies between about 90% for a minimum MAPMT radial position of 280mm and 60% for the maximum radial position of 400mm. The main goals of these measurements are:

- study in details the Cherenkov angle resolution, also by varying the aerogel thickness and refractive index;

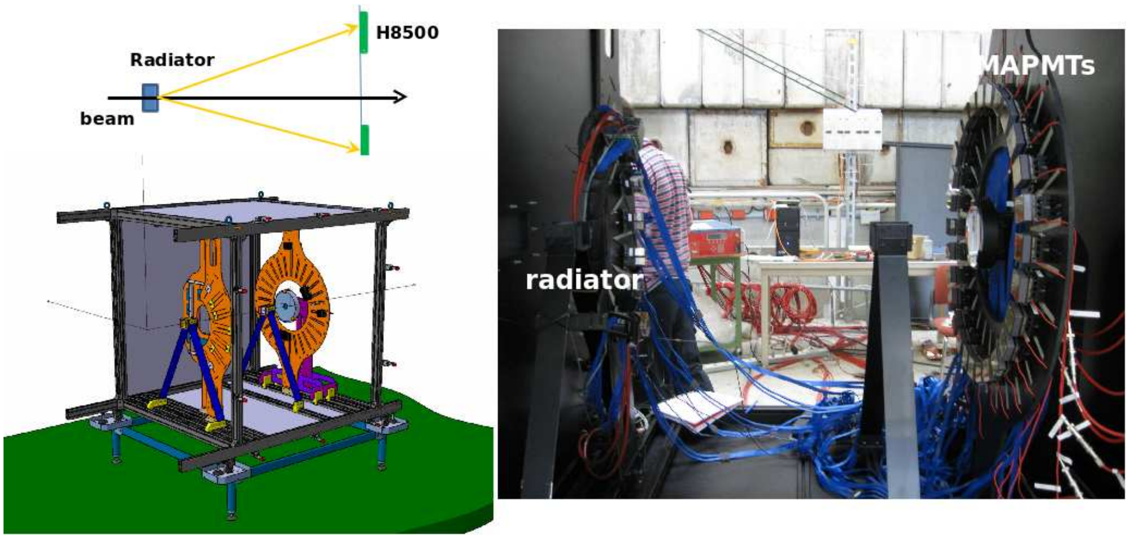

Figure 2: Top left: concept of the direct light measurements. Bottom left: drawing of the prototype. Right: picture of the prototype.

- measure the π/K separation up to 8 GeV/c;
- estimate the pion detection efficiency;
- study the backgrounds, in particular from Rayleigh scattering.

In Fig. 3, we show the setup for the reflected light measurements. In this case, the aerogel support is placed closer to the MAPMTs plane, then we have a spherical mirror wich reflects the Cherenkov photons back toward a system of eight squared planar mirrors (dimensions 10.5×10.5 cm^2) which send the light to the MAPMTs. The MAPMTs are mounted on a support similar to the one used for the direct light, but optimized to better match the coverage of the planar mirrors and the bigger Cherenkov ring radius due to the larger photon path. The ring coverage runs from about 75% (minimal radial position of 350 mm) to 50% (maximal radial position of 540 mm). The planar mirrors may be moved longitudinally to optimize the total gap length with respect to the focal lenght of the spherical mirror and to maximize the focussing of the light cone. The supports of the planar mirrors are designed to allow the insertion of tiles of aerogel, in order to study the photon yield absorption within the aerogel.

For these measurements, the main goal is the study of the depletion in the photon yield due to the multiple passes of the Cherenkov photons in the aerogel, namely:

- compare runs without or with aerogel absorber in front of the planar mirrors;
- optimize the aerogel thicknesses;
- compare the optical quality of different mirrors.

Additionally, one could also study the π/K separation and the detection efficiencies. However, we must stress that the geometry of the prototype is different from that of the

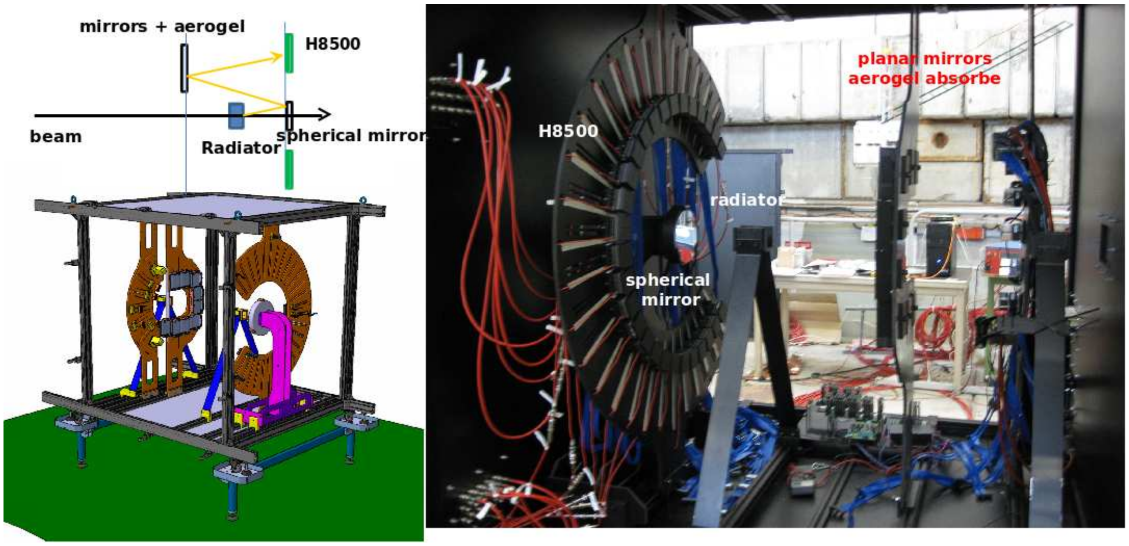

Figure 3: Top left: concept of the reflected light measurements. Bottom left: drawing of the prototype. Right: picture of the prototype.

CLAS12, thus the results we have obtained will not be indicative of the final RICH performances. On the other hand, they will be used to tune the Monte Carlo simulations, that ultimately will provide us the expected performances of the detector.

The setup is completed by two planar Gas Electron Multiplier (GEM) chambers, installed outside of the RICH box, for tracking of the incoming particles, and by a gaseous threshold Cherenkov detector (part of the T9 equipment), used to make offline selection of pure pion or heavier hadron beam. Finally, two small plastic scintillators were placed at the end of the beam line, just after the second GEM chamber, to define the trigger signal of the DAQ system.

3 The T9 beam line at CERN

The main tests of the RICH prototype have been performed at the T9 beam line located in the East Area of the PS/SPS complex at CERN. The primary proton beam is sent to a target to produce a secondary beam. Different targets, magnets and collimators allow to select the composition of the secondary beam (electrons, muons or hadrons), the charge and the momentum (from 3 to 8 GeV/c). In our test, we run with the hadron target with negative charge (see the hadron intensities in Fig. 4) and momentum between 6 and 8 GeV/c, the maximum range covered by CLAS12.

The time structure of the beam was determined by the extraction of one or more spills from the primary PS proton beam. Each spill had a duration of 400ms and the period of the PS operation was 40 s, so that overall the duty cycle was of the order of few percent.

From Fig. 4, we estimated in our beam a relative population of $\pi^- : K^- : \bar{p}$ of 160 : 4.5 : 1, approximately independent from the momentum in the range between 6 and 8 GeV/c.

The T9 standard equipment included a gas Cherenkov counter that has been used to

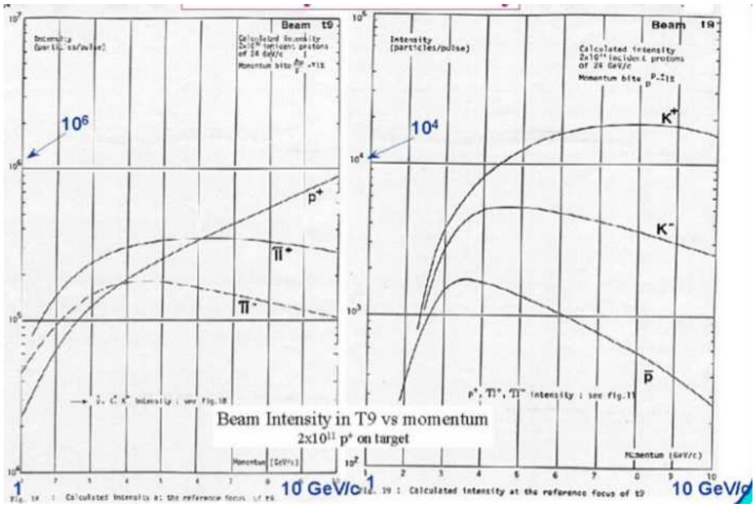

Figure 4: Hadron intensities as a function of the momentum in the T9 configuration of our tests.

separate pions from heavier hadrons by adjusting the gas pressure so that only pions were above threshold. A sample ADC spectrum is shown in Fig. 5, where we see a broad distribution due to the pions and a narrow pedestal peak of below-threshold hadrons. Cut at 150 channel (5σ above the pedestal peak) is set to separate pions from other hadrons.

4 Electronics and DAQ

The prototype was made by 28 MAPMTs for a total of 1792 channels. They were readout through a MAROC3 chip [7], a 64-channel ASIC which provides charge measurement (up to 5 pC) for signal greater than 1/3 photoelectron, with a linearity of 2% or better and a crosstalk less than 1%. Each MAROC3 chip was mounted on a front-end (FE) card connected to the MAPMT through a flat cable. The 28 FE cards were installed on a number of back-plane (BP, each of them may host up to 16 cards), connected to two control boards (CB). The total available channels are 4096 in a very compact system. The various components and the assembled set-up are shown in Fig. 6.

The GEM were readout using APV25 cards, which allow the analysis of the pulse shape of each strip by sampling the signals at fixed time intervals. Each card has 128 channels, thus one GEM wss read by 2 APV card per side. The system was completd with a CAEN V785N ADC for the threshold Cherenkov readout. The DAQ software managed the acquisition of the different systems through a CAEN VME bridge V2718, connected to the computer via optical link.

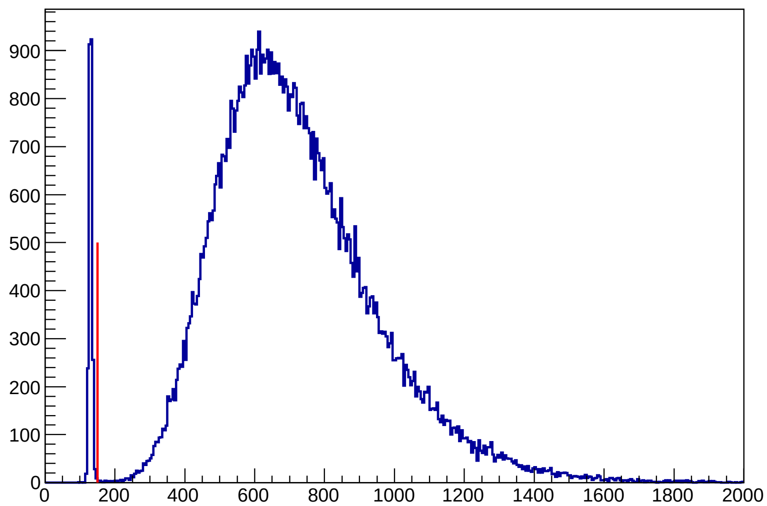

Figure 5: Typical ADC spectrum of the threshold Cherenkov counter. The red line indicates the threshold to separate pions from heavier hadrons.

Figure 6: Left plot: the various components of the MAROC3 electronics. Right plot: the assembled setup installed in the RICH prototype box.

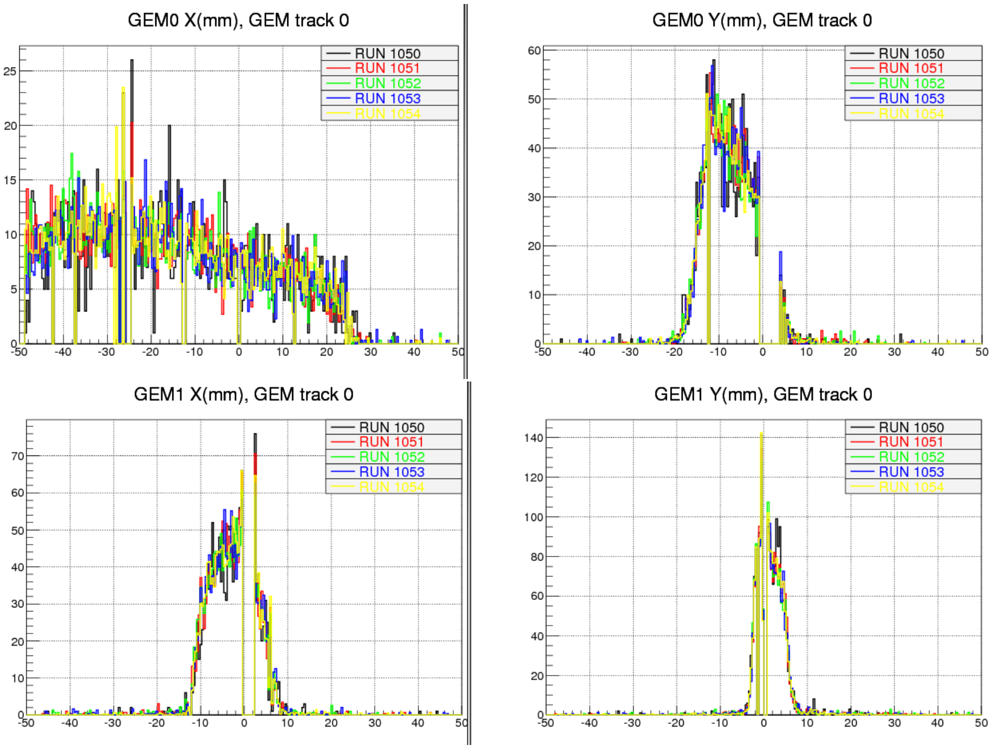

Figure 7: Horizontal and vertical beam profiles measured on GEM0 (upstream to the RICH, top plots) and GEM1 (downstream to the RICH, bottom plots).

5 Track reconstruction

Particle's trajectories are measured through two GEM chambers, placed about 4 meters far each other, with the downstream one about 80 cm after the MAPMT plane. Each chamber is 10×10 cm^2 and is readout in 256 strips for both x and y. In each event, the strip signals are sampled three times at 20ns intervals, thus good signal are searched for by looking at peaks in the strip ADC distributions of all the 3 samples. In addition, one may require correlation between the amplitudes of the signals measured in the two planes of one GEM. A good GEM hit is obtained by any pair of signals measured on the two planes of one chamber. A good GEM track is reconstructed by matching one hit on the first GEM with one hit on the second GEM.

The beam profiles measured in the two GEM chambers are shown in Fig. 7 for several different runs over the data taking period. The holes in the distributions are due to noisy strips that have been removed in the off-line analysis. The measured profiles don't show any significant modification across the test period, thus ensuring the stability of the beam conditions and of the tracking system. The profile is wider on GEM0 (upstream GEM) because of the focussing of the beam. Part of the beam on the horizontal plane was missing, resulting in a decreased tracking efficiency. There is also a different beam collimation in X and Y, so that the horizontal width is about twice the vertical one.

A typical distribution of the number of tracks per event is shown in Fig. 8. Most of the

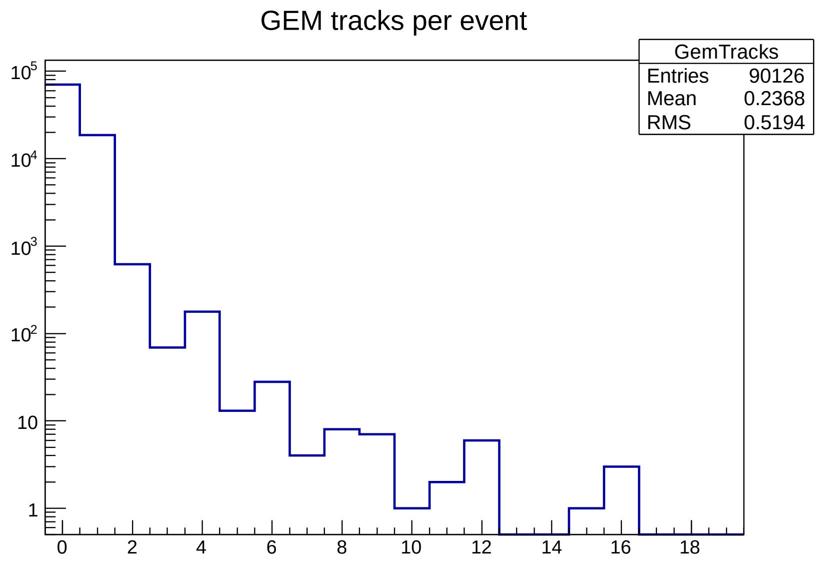

Figure 8: Number of GEM tracks per event.

events have no good tracks, because of the tight cuts used for the reconstruction and also because of the partial beam coverage of the first GEM. When more than one track in the event is found, only the one obtained from the biggest strip signals is retained. The average GEM efficiency is of the order of 30%.

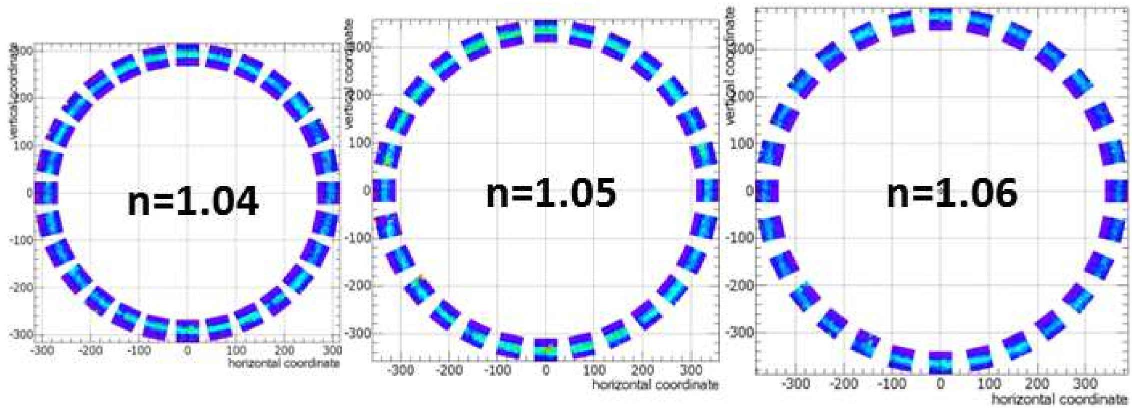

Figure 9: Cherenkov photon hit pattern measured with aerogel of different refractive index.

6 Ring reconstruction

In the prototype configurations, for the direct as well as for the reflected light measurements, the expected Cherenkov photon patterns are rings centered on the projection of the particle's track onto the MAPMTs array plane. MAPMT hits are identified by applying a 5σ cut above the pedestal peak. Examples of the measured hit distributions for different aerogel refractive index is shown in Fig. 9.

The Cherenkov rings are reconstructed by minimizing the quantity

$$S(R, X_C, Y_C) = \sum_{i=1}^{N_{pe}} [(x_i - X_C)^2 + (y_i - Y_C)^2 - R^2]^2 \tag{1}$$

where (x_i, y_i) are the coordinates of the i_{th} photon hit, (X_C, Y_C) are the coordinate of the ring center and R its radius. The minimization can be performed either analitically or using MINUIT.

The Cerenkov angle is then calculated from the known distance D between the MAPMT plane and the center of the aerogel radiator from

$$\tan(\theta_C) = \frac{R}{D} \tag{2}$$

In the analysis, one can make the ring reconstruction using only the MAPMTs array, fitting at the same time the center coordinates and the radius (a *3par* fit), or using the center information from the GEM track and fitting only the radius (a *1par* fit). In the latter case, a better resolution is expected, because of the reduced number of free parameters. Comparison between the two fits have been used as a validation of the GEM track reconstruction.

In principle, in the *3par* fit 3 hits are sufficient to reconstruct the ring, while in the *1par* fit just one would be enough. However, with such small number of hits the background may lead to uncorrect particle identification, thus a minimum number of 4 hits is always required.

In Fig. 10, we show for example the hit distribution of one event measured with $n = 1.05$ and $t = 2$ cm aerogel, together we the fitted ring. We can identify in this event 12 good hits

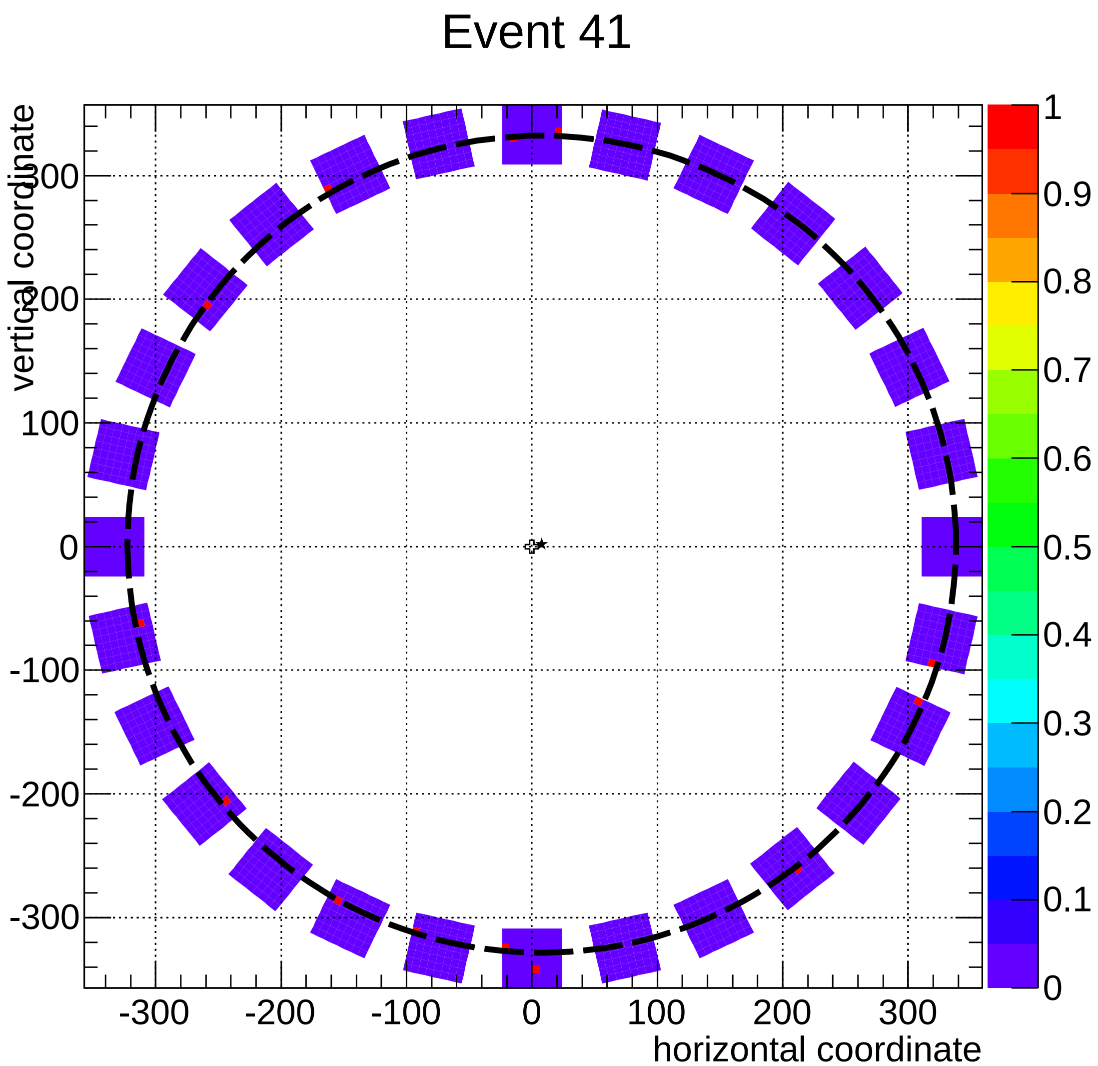

Figure 10: Hit distribution of one event measured with $n = 1.05$ and $t = 2$ cm aerogel. The circle show the Cherenkov ring fitted to the hits.

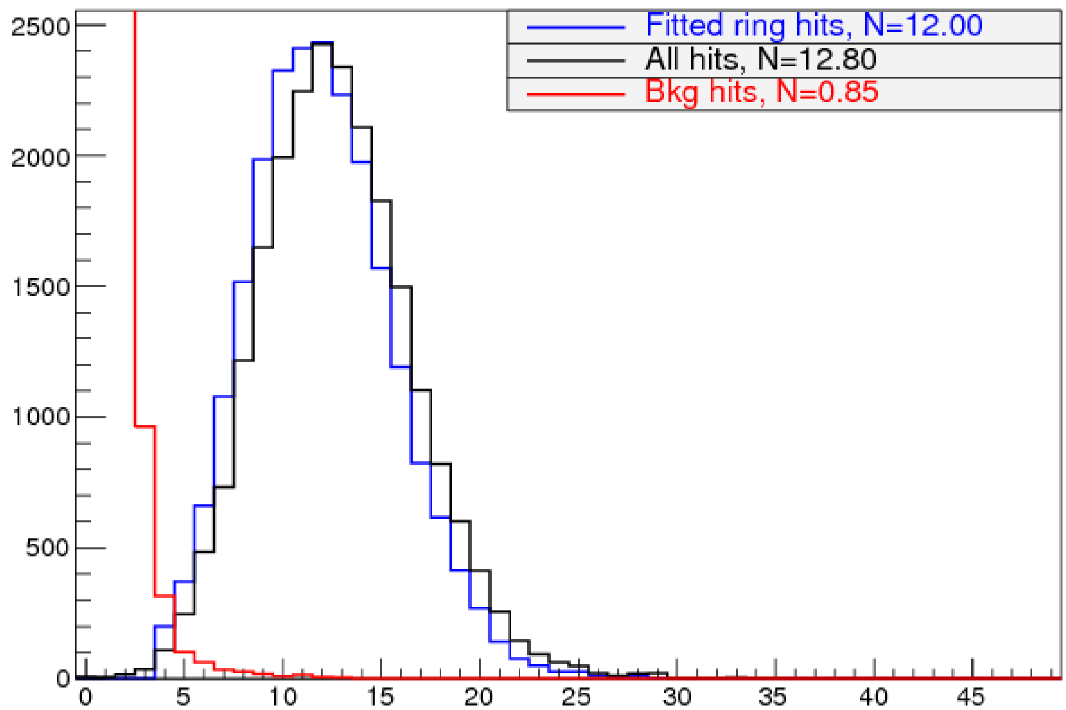

Figure 11: Number of MAPMT hit per event: all hit above threshold (black histogram), background hits (red histogram) and Cherenkov hit (blue histogram). Mean values of the distributions are reported in the legend.

laying on the ring, plus one hit (in the bottom center MAPMT) far enough from the ring that can be considered as background. Thus, an iterative procedure has been implemented in order to suppress background hits. A hit is considered as background if its distance from the fitted ring is bigger then some cut. In this case, the hit is removed and a new fit is performed taking into account only the remaining good Cherenkov hits. The cut value has been optimized to the data. In fact, a too loose cut will include too many background hits, thus worsening the resolution, while a too tight cut will remove good photons, again worsening the resolution. An optimal value of 12mm has been found. In Fig. 11, the total number of hits (black histogram), background hits (red histogram) and Cherenkov hits (blue histogram) are shown. On average, with respect to about 12 Cherenkov hits, we have less than 1 background hits per event. Taking into account the total number of channels in the ring region, it corresponds to a dark count rate of about 10^{-4}.

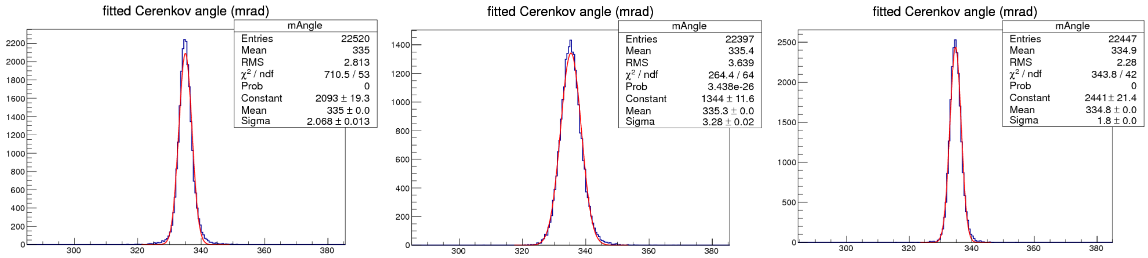

Figure 12: Cherenkov ring radius from the *3par* fit (left), from the *1par* fit before (center) and after (right) the GEM alignment procedure.

GEM	X_{GEM} (mm)	Y_{GEM} (mm)
0	-0.32±0.12	0.00±0.13
1	-9.14±0.03	1.04±0.02

Table 1: GEM alignment constants.

7 GEM alignment

Rough alignment of the GEM chambers was done during the installation of the setup. A finer alignment has been obtained off-line by fitting the GEM tracks to the ring reconstruction.

A set of alignment $X_{GEM0}, Y_{GEM0}, X_{GEM1}, Y_{GEM1}$ constants has been introduced to take into account possible displacements of the GEM on the transverse plane with respect to the beam line. These displacements have been determined by minimizing the quantity:

$$Q(X_{GEM0}, Y_{GEM0}, X_{GEM1}, Y_{GEM1}) = RMS(R) + Mean^2(\Delta X) + Mean^2(\Delta Y) \quad (3)$$

where $RMS(R)$ is the RMS of the distribution of the Cherenkov ring radius in the *1par* fit and $Mean(\Delta X)$ and $Mean(\Delta Y)$ are the mean values of the distributions of the difference between the GEM track (projected on the MAPMT plane) and the ring center coordinates obtained in the *3par* fit. In Fig. 12, we show the Cerenkov angle distribution from the *3par* fit (left, $\sigma = 2.1$ mrad), from the *1par* fit before (center, $\sigma = 3.3$ mrad) and after (right, $\sigma = 1.8$ mrad) the offline alignment. An improvement of more than 10% in the ring resolution has been obtained from the *3par* to the *1par* fit. The stability of the procedure has been checked by calculating the alignment constants from several runs with different beam energies, as shown in Fig. 13. The six runs at $P = 8$ GeV/c have been taken at the beginning and the runs at $P = 6, 7$ GeV/c at the end of the data taking, but no major differences have been found. The final alignment constants are reported in Tab. 1.

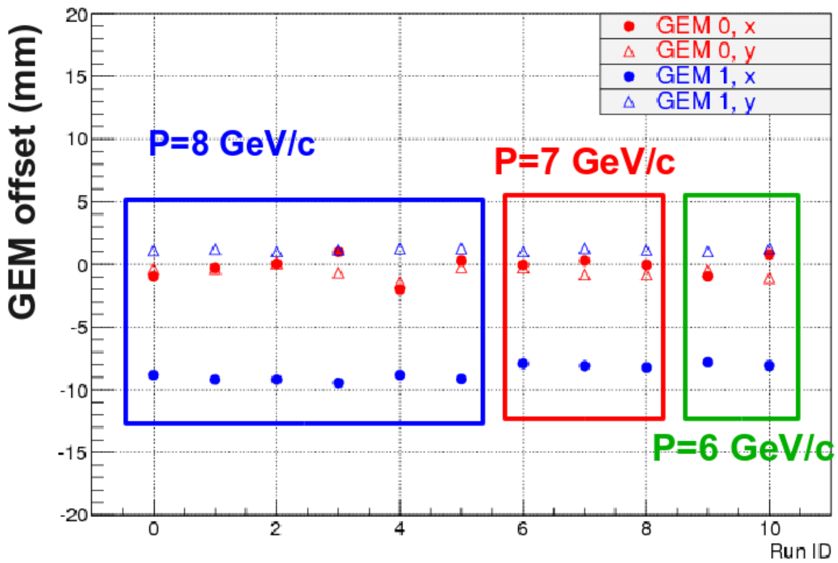

Figure 13: GEM alignment constants for various runs at different beam energies.

8 Direct light measurements: pions and kaons

We report here the main results of the measurements with the direct light configuration, discussing the pion and kaon reconstruction and separation. Because of the geometry of the prototype very close to the one of the CLAS12 RICH, we consider these results as a good estimate of the performance of the final detector.

Our reference run conditions have aerogel with nominal refractive index $n = 1.05$ and $t = 2$ cm thickness and beam with $P = 8$ GeV/c, the highest reacheable in the CLAS12 RICH. Our Cherenkov ring reconstruction is performed with a *1par* fit using the GEM alignment constants in Tab. 1. We select events with at least 4 MAPMT Cherenkov hits (after background subtraction).

8.1 Pion Reconstruction

Pion events are selected by requiring a gas Cherenkov counter signal above threshold, see Fig. 5.

In the left panel of Fig. 14, we show a scatter plot of the Cherenkov angle versus the number N_{pe} of photoelectrons. It is clear that the distributions get narrower as N_{pe} increases. For a fixed number of N_{pe}, the angle distribution has been fitted with a gaussian to extract mean and width. The mean values don't show any appreciable deviation from the one obtained in the integrated fit (see Fig. 12 right). The gaussian widths are expected to follow the statistical law:

$$\sigma_\theta = \frac{\sigma_{1pe}}{\sqrt{N_{pe}}} \tag{4}$$

where σ_{1pe} is the single photon detection resolution, that can be decomposed in contribution from pixel size (σ_{pix}), chromatic effects (σ_{chr}) and emission point uncertainty (σ_{emi}):

$$\sigma_{1pe}^2 = \sigma_{pix}^2 + \sigma_{chr}^2 + \sigma_{emi}^2 \tag{5}$$

To take into account possible spurious contributions, the results in the right plot of Fig. 14 has been fitted with the function

$$\sigma_\theta = \sigma_0 + \frac{\sigma_{1pe}}{\sqrt{N_{pe}}} \tag{6}$$

The fit gives a constant term compatible with zero and a single photon resolution $\sigma_{1pe} = 5.90 \pm 0.03$ mrad.

We now assume as identified pions those events with an angle within $\pm 3\sigma$ around the mean value, with the σ given by the fit in the right plot of Fig. 14. We then calculate the pion detection efficiency as the ratio between the number of identified pions and the number of events with gas Cherenkov counter signal above threshold. We obtain $\epsilon(\pi) = 98.4 \pm 0.1\%$. No beam energy dependence has been found.

8.2 Kaon Reconstruction

Events below the gas Cherenkov counter threshold includes both kaons and antiprotons. In Fig. 15, we compare the Cherenkov angle distributions measured for these events (red

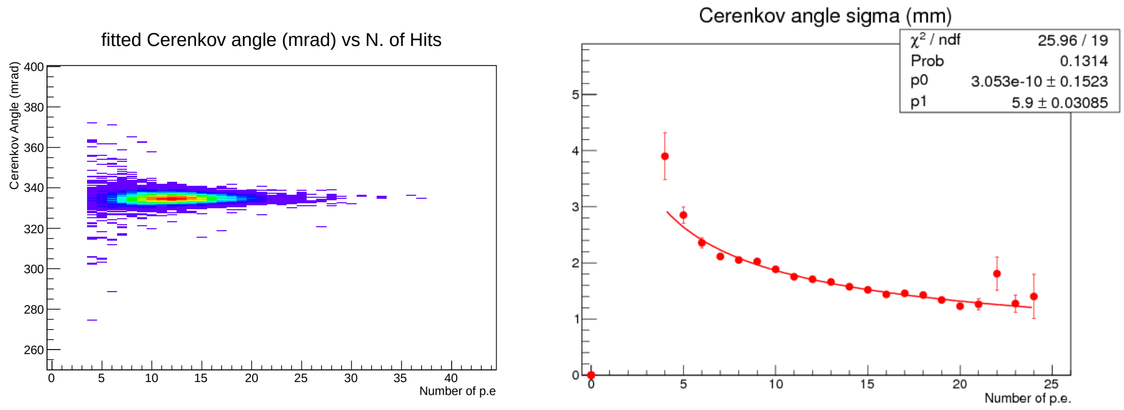

Figure 14: Data with $n = 1.05$ and $t = 2$ cm. Left plot: Cherenkov angle versus the number N_{pe} of photoelectrons. Right plot: gaussian width of the Cherenkov angle distribution as a function of N_{pe}.

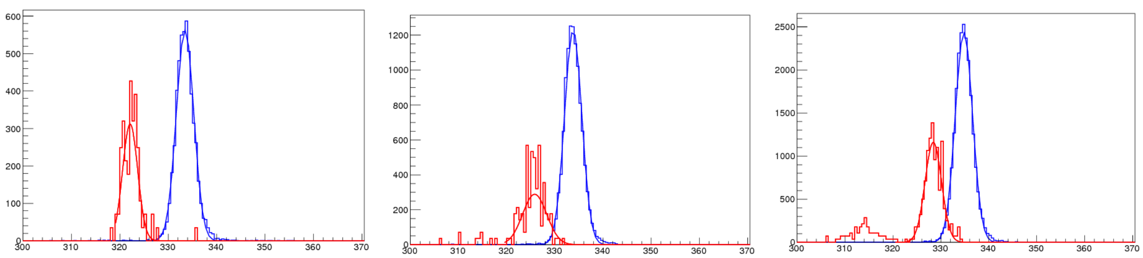

Figure 15: Pion Cherenkov angle distributions (in mrad, blue histograms) compared with those from events with gas Cherenkov signal below threshold (red histograms), for $P = 6, 7, 8$ GeV/c beam (from left to right).

histograms) with the distributions for pions (blue histograms) at the three beam energies $P = 6, 7, 8$ GeV/c, from left to right. The red histograms are rescaled by the relative beam intensities (see Sect. 3). We see the prominent kaon peak separated from the pion one and, at the highest energy, some tail of the $\bar{p}$ peak, wich disappears as the energy decreases because it goes out of the MAPMTs radial coverage. In Tab. 2, we report the mean and width of the gaussian fits of the pion and kaon angles. We define the number of σ separation between kaon and pion as:

$$n_\sigma = \frac{\theta_C(\pi) - \theta_C(K)}{[\sigma_\theta(\pi) + \sigma_\theta(K)]/2} \tag{7}$$

and we obtain the values showed in the last column of Tab. 2. Here, we assumed $\sigma_\theta(K) = \sigma_\theta(\pi)$ to avoid the large fluctuations in the value of $\sigma_\theta(K)$ due to the small kaon statistics. Up to the highest momentum, it is always $n_\sigma > 3$.

To calculate the kaon efficiency, we need to know the number of incoming kaons in the beam. From Fig. 4, the K/π flux ratio may be estimated only approximatively, thus we used a statistical analysis of the measured photon yield. We consider for example the highest beam energy, $P = 8$ GeV/c, and we apply a cut $R > R_{min}(K) = 323$mm to separate kaons from $\bar{p}$. In Fig. 16, we show the number of Cherenkov photon hits per event measured

P (GeV/c)	$\theta_C(\pi)$ (mrad)	$\sigma_\theta(\pi)$ (mrad)	$\theta_C(K)$ (mrad)	$\sigma_\theta(K)$ (mrad)	n_σ
6	333.47±0.03	1.81±0.02	322.13±0.04	1.56±0.04	6.3
7	333.79±0.02	1.79±0.02	325.79±0.05	2.50±0.05	4.4
8	334.80±0.01	1.80±0.01	328.41±0.02	1.72±0.02	3.5

Table 2: Gaussian mean and width of pion and kaon Cherenkov angles and number of σ separation, the latter computed assuming $\sigma_\theta(K) = \sigma_\theta(\pi)$.

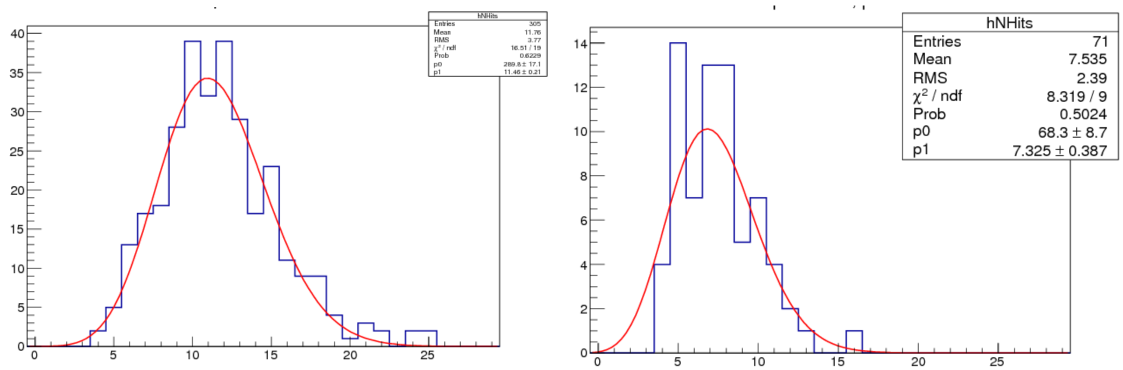

Figure 16: Number of Cherenkov hits per event for kaons (Left) and antiprotons (right).

for the kaons (left) and for $\bar{p}$. The histograms are fitted with a Poisson curve in order to estimate the fraction of events with less than four hits, the minimum required for the ring reconstruction. While this fraction is basically negligible for kaons, we obtain a correction of about 7% because of the lower Cherenkov photon yield produced by $\bar{p}$. After this correction, we obtain a relative rate of 4.3 : 1 between kaons and antiprotons, in good agreement with the expectations from Fig. 4.

The pion and kaon peaks partially overlap, especially at the highest beam energy. Thus, to suppress the pion contamination, we consider as identified kaons those events with

$$\theta_C^{min}(K) < \theta_C < \theta_C^{min}(\pi) \tag{8}$$

where $\theta_C^{min}(\pi) = \theta_C(\pi) - 3\sigma_\theta(\pi)$ and the pion ring width $\sigma_\theta(\pi)$ is the N_{pe}-dependent one of the fit in Fig. 14. The efficiencies, for both pions and kaons, are reported in Tab. 3.

P (GeV/c)	$\epsilon(\pi)$ (%)	$\epsilon(K)$ (%)
6	98.1±0.2	99±2
7	98.3±0.1	95±2
8	98.8±0.1	67±3

Table 3: Pion and kaon detection efficiencies measured at three momenta. The errors are statistical only.

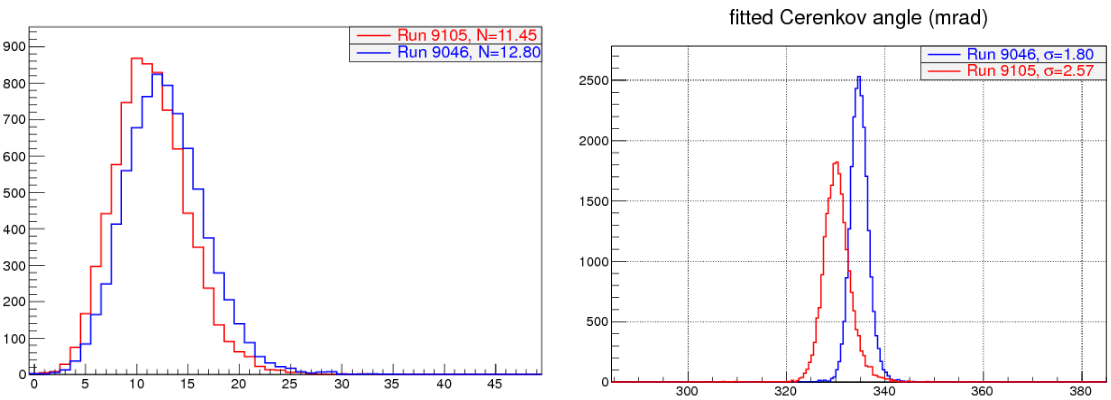

Figure 17: Left plot: number of hits per event with old (red histogram) and new (blu histogram) aerogel production, for tiles with $n = 1.05$ and $t = 2$ cm. Right plot: same comparison for the Cherenkov angle distributions.

9 Direct light measurements: systematic studies

In this section, we discuss several systematic measurements performed varying the aerogel radiator as well as the MAPMT configuration. On one side, they will be used to tune the Monte Carlo simulation of the CLAS12 RICH, on the other side they will give us information on the improvements that can be obtained in the final detector.

9.1 New vs old aerogel production

During the test, we ran with aerogel belonging to various production over more than one year. In fig. 17, we compare the ring radius reconstruction for one "CERN-6" tile and one of the "Tiles", both with refractive index $n = 1.05$ and thickness $t = 2$ cm. In the left plot, we compare the number of hits, showing that the aerogel from the newer production produces on average about one hit more. In the right plot, we compare the Cherenkov angle distributions. We see a clear improvement in the resolution with the new aerogel (about 40% improvement in the σ_θ) but also a mean value of the Cherenkov angle differing by about 4 mrad, because of slightly smaller refractive index of the older aerogel with respect to the nominal value $n = 1.05$.

9.2 UV photons

The array of MAPMTs include 14 with normal glass window H8500C and 14 with UV-enhanced glass window H8500C-03, alternated along the ring. The effect of the UV photons can be estimated by comparing the photon yield and Cherenkov angle resolution using only the MAPMTs of the same type. In Fig. 18, we show the distributions of the number of MAPMT hits (left plot) and of the residuals, i.e. the distance between the hit and the ring (right plot). The red histograms refer to normal glass MAPMTs and the blue ones to the UV-enhanced glass. The latter have on average one hit more, but the residual distribution

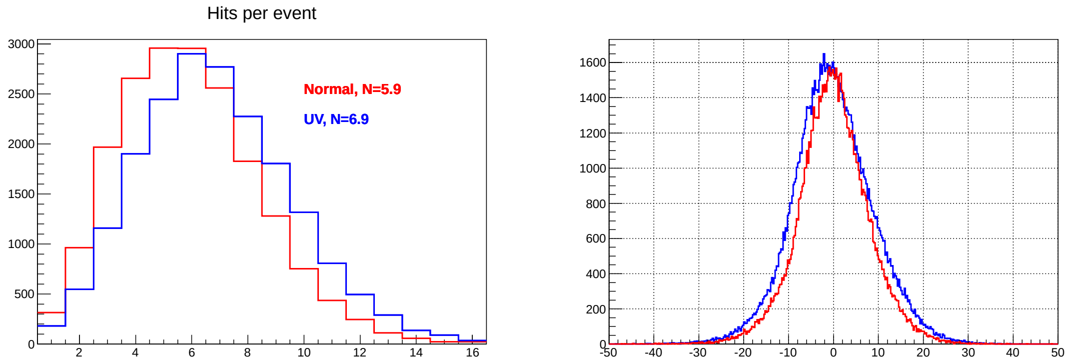

Figure 18: Left plot: number of hits per event with normal glass (red histogram) and UV-enhanced glass (blu histogram) MAPMTs. Right plot: same comparison for the residuals.

	σ_{1pe} (mrad)
14 H8500C	5.07±0.21
14 H8500C-03	6.53±0.04
All 28	5.90±0.03

Table 4: Single photon resolutions of the Cherenkov angle for the various type of MAPMTs.

is sigificant broader and slightly off from zero. This is due to the bigger scattering of the UV photons before reaching the MAPMTs. The result is that, tough having one Cherenkov hit less, the resolution is better using the normal glass, as shown by Fig. 19, where the gaussian width of the Cherenkov angle as a function of N_{pe} for the two types of MAPMT is compared with the one obtained using all the 28 MAPMTs. In Tab. 4, we report the extracted values of the single photon resolution. Overall, the H8550C-03 have a resolution about 30% worse than the H8500C.

9.3 Chromatic effect studies

The Cherenkov ring resolution has been studied as a function of the photon wavelength by applying optical filters just after the aerogel radiator. Data have been aquired with $n = 1.05$ nominal refractive index and $t = 2$ cm thickness aerogel and the set of available filters allowed to span the entire range of relevant wavelengths, from UV to the red. The Cherenkov ring radius measured as a function of the wavelength λ is shown in Fig. 20 as red points. The variation of the radius reflects the variation of the refractive index with the wavelength, of the order of 0.1% maximum from the UV to the infrared ranges.

Knowing the Cherenkov ring radius at a given wavelength, one can estimate the variation of n with λ. The experimental points have been fitted by using the dispersion law of eq. [5] and taking into account the diffraction of the Cherenkov photons when they cross the surface between the aerogel and the air and between the air and the filters. The result is shown

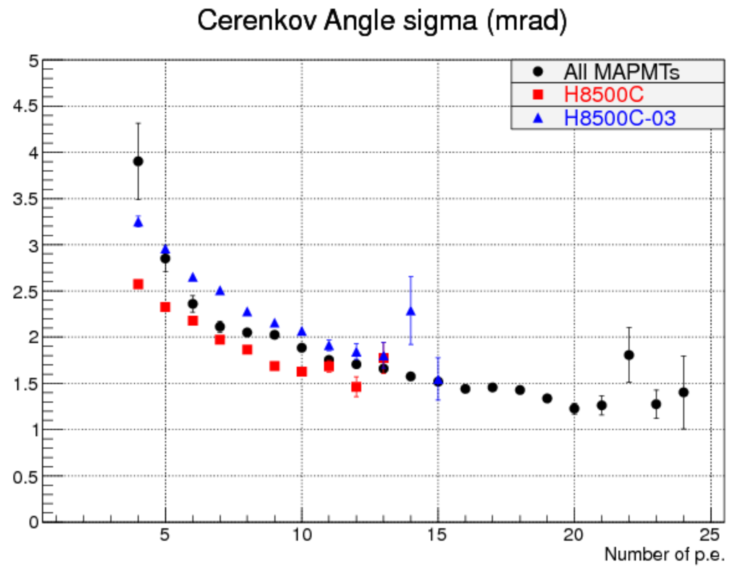

Figure 19: Gaussian width of Cherenkov ring radius as a function of N_{pe} measured with 14 UV-enhanced glass MAPMTs (blue triangles), with 14 normal glass MAPMTs (red squares) or with all the 28 MAPMTs (black circles).

in Fig. 20 by the full line. It well reproduce the measured data. The small point-by-point fluctuations of the curve are due to the different thickness of the various filters used. On the top of the figure, the values of the fitted parameters $P1$ and $P2$ of equation [5] are reported. By comparison, the values measured using the spectrophototmeter [6] are:

$$P1 = 0.0899 \pm 0.0001\text{n}m^{-2}$$

$$P2 = 60.92 \pm 1.65nm$$

in good agreement with the results of the Fig. 20. The fit gives at $\lambda = 400$ nm the value of the aerogel refractive index $n = 1.049$.

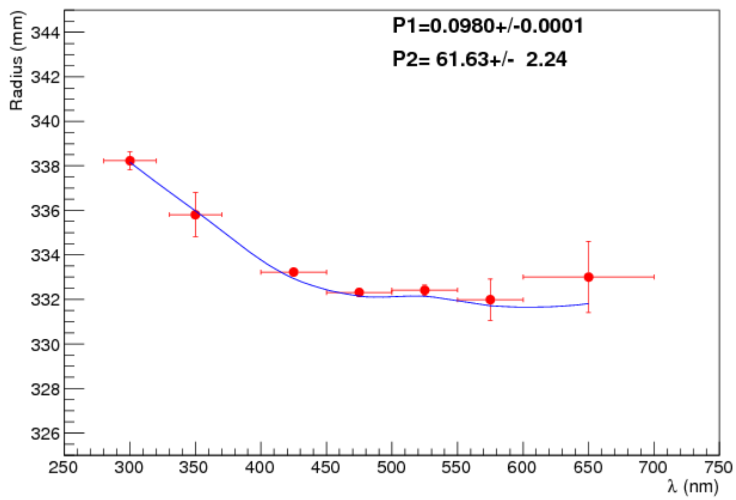

Figure 20: Measured Cherenkov ring radius as a function of the wavelength with $n = 1.05$ nominal refractive index and $t = 2$ cm aerogel. The curve is a fit of the data as described in the text.

10 Reflected light measurements

For these measurements we ran with two different curved mirrors, a glass spherical one and a composite elliptical one, produced at JLab as a prototype for the HTCC. The setup (see Fig. 3) was completed by the aerogel radiator placed about 20 cm before the curved mirror and a set of eight planar mirrors, in front of which tiles of aerogel could be placed.

Though similar in the concept, this configuration is not the same as for the CLAS12 RICH. In fact, the gap lenght is much smaller (about 1.3m vs 3m) and it was not possible to put the MAPMTs on the focal plane of the mirrors. In addition, the relative alignment of the mirror system with the prototype box was checked only at a few mm level and a relative off-line alignment of the various elements was performed using the Monte Carlo simulations. Thus, we expect to obtain from the prototype measurements a worse ring reconstruction resolution than in the CLAS12 RICH. However, the results will be used to tune the Monte Carlo simulations from which we will estimate the RICH resolution.

We run with beam momentum of 6 GeV/c and in the nominal configuration we had aerogel radiator with refractive index $n = 1.05$ and thickness $t = 6$ cm. Data were recorded with and without aerogel absorbers in front of the planar mirrors. Here we used tiles with $n = 1.05$ and $t = 2$ cm, five from the latest production (the "CERN" in Tab. [2]) and three from a previous production (the "Sample" in Tab. [2]).

Because of the difficulty in estimating the total photon path length after the mirror reflections, we show in this section the results in terms of ring radius instaed of Cherenkov angle.

10.1 Results with the spherical mirror

The spherical mirror, produced by the Marcon company was made of glass, had a diameter of 25cm and a focal lenght of 90 cm. In Fig. 21, we show the number of hits per event with and without the absorbers. We have 13.1 p.e. without absorber and 5.3 with absorber, with a yield loss of about 60%.

The ring radius reconstrution for the two measurements is compared in Fig. 22. In the left plot, we compare the radius distribution measured without absorber with the results with the absorber. We see a worsening of the resolution, with $\sigma_R = 2.67 \pm 0.01$ mm without and $\sigma_R = 3.79 \pm 0.02$ mm with the absorbers. This is largely due to the decrease in the number of p.e. The resolutions as a function of the number of p.e. is shown in the right plot of Fig.22. While without absorber there are events up to $N_{pe} = 20$, with the absorbers the maximum value with significant statistics is $N_{pe} = 11$. On the contrary, the fitted single photon resolution doesn't change significantly, since we obtained $\sigma^R_{1pe} = 9.55 \pm 0.04$ mm and $\sigma^R_{1pe} = 9.25 \pm 0.04$ mm without and with the absorbers, respectively. This is quite an important results.

The kaon/pion separation power is shown in Fig. 23 without (left plot) and with (right plot) the aerogel absorbers. The red histograms show the ring radius for pions and the blue one for kaons and the parameters of the gaussian fits are reported in Tab. 5. The estimated separations using eq. 7 are reported in the last column of the table. Though they are below the required values, they are a remarkable result and their relation will the expected CLAS12 RICH performances will be discussed in Sect. 12.

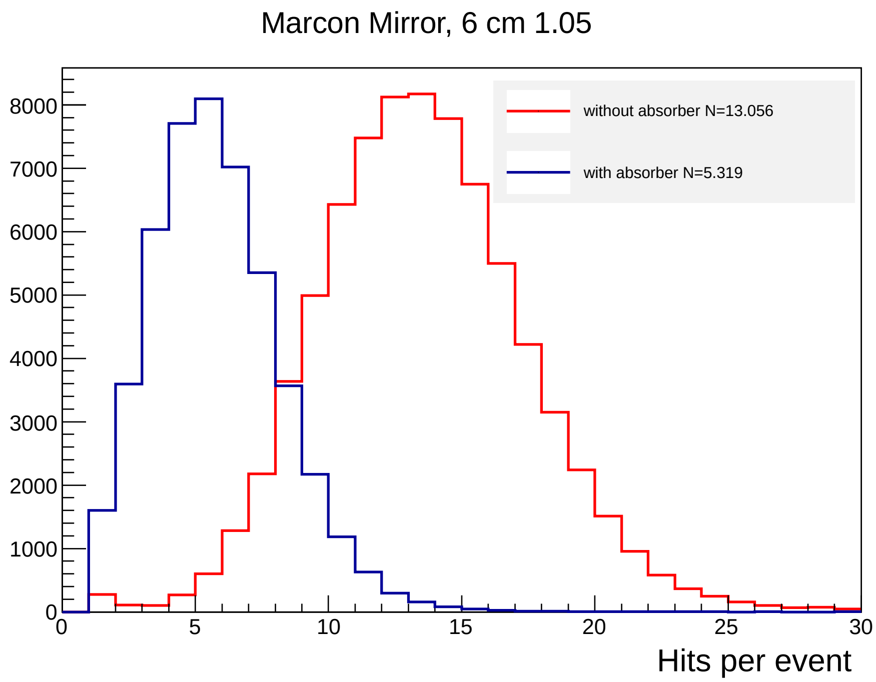

Figure 21: Number of hits per event for data without the aerogel absorber (red histogram) and with the 2cm aerogel absorbers placed in front of the planar mirrors (blue histogram).

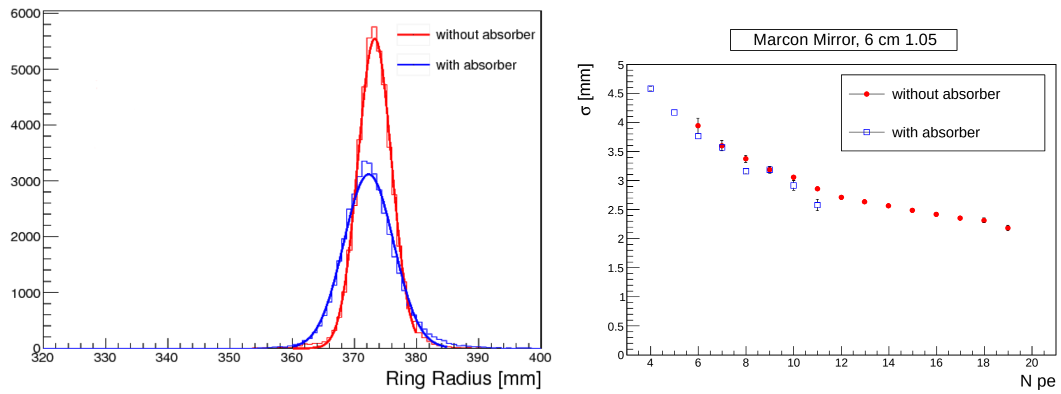

Figure 22: Left plot: ring radius distributions without (red histogram) and with (blue histogram) the aerogel absorber. Right plot: gaussian width of the ring radius as a function of the number of $p.e.$ for runs without (black circles) and with (red circles) the aerogel absorbers.

Absorbers	$R(\pi)$ (mm)	$\sigma_R(\pi)$ (mm)	$R(K)$ (mm)	$\sigma_R(K)$ (mm)	n_σ
NO	373.31±0.01	2.67±0.01	364.31±0.01	2.82±0.01	3.3
YES	372.19±0.01	3.79±0.02	363.29±0.01	3.18±0.01	2.5

Table 5: Gaussian mean and width of pion and kaon Cherenkov ring radius and number of σ separation fro the reflected light measurements.

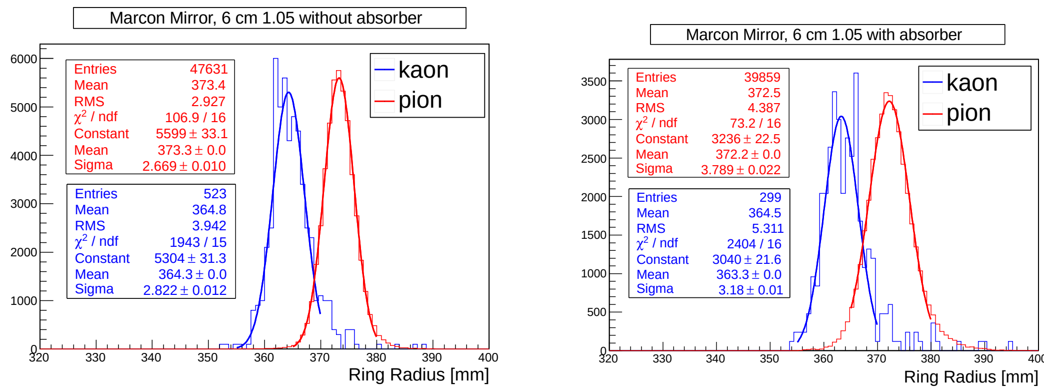

Figure 23: Pion (red histograms) and kaon (blue histograms) ring radius distributions without (left plot) and with (right plot) aerogel absorber in the reflected light data with aerogel radiator with $n = 1.05$ ad $t = 6$ cm.

Absorbers	Marcon	JLab
NO	13.38±0.04 mm	14.64±0.06 mm
YES	16.24±0.07 mm	17.29±0.07 mm

Table 6: Single photon resolution σ^R_{1pe} of the Cherenkov ring radius extracted from reflected light data with and without aerogel absorbers for Marcon (spherical) and JLab (elliptical) mirrors.

10.2 Comparison with the JLab mirror

We made masurements also using an elliptical mirror produced at JLab placed instead of the spherical one. This mirror had focal lengths $f_x = 1848$ mm and $f_y = 1613$ mm, cut in a rectangular shape of approximately 533×361 mm^2. Comparison between the results with the two different mirrors have been done in order to have a first rough estimate of the performance of a mirror of similar type to the ones that will be used in the CLAS12 RICH. Due to the complications in checking the alignment of this mirror with respect to the beam line and to the asymmetry produced in the Cherenkov ring, this comparison will be performed by doing a *3par* fit, i.e. without using the GEM tracking information. When fitting the ring, a rescaling of the horizontal and vertical coordinates of +4% and −4% has been applied, in order to take into account the elliptical shape of the mirror surface.

The number of p.e. with two mirrors are compared in Fig. 24 without (left plot) and with (right plot) aerogel absorbers. No significant differences have been found. The single photon resolutions σ^R_{1pe} are compared in Tab. 6. The numbers are very close, with the composite JLab mirror having a slightly (about 1 mm) worse resolution.

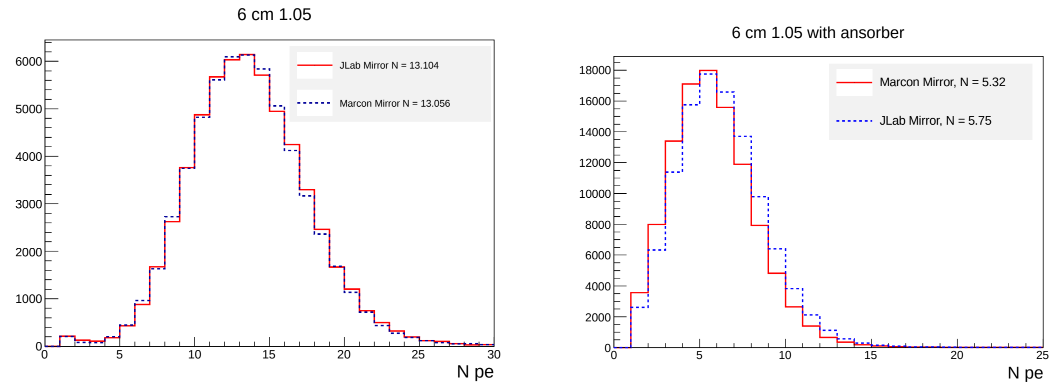

Figure 24: Number of p.e. per event using JLab composite (red full histograms) and Marcon glass (blue dashed histograms) mirrors: results without (left plot) and with (right plot) aerogel absorbers.

11 Monte Carlo comparison

The setup used in the CERN test beam has been implemented in a Monte Carlo using the same **GEANT4** package used in the simulation of CLAS12. Several parameters of the simulations required a fine tuning to match the test beam results. After this process, a satisfactory agreement between the simulation and the test beam data has been obtained, thus allowing to apply the Monte Carlo code to simulate the response of the CLAS12 RICH with confidence that the results will be a reasonable estimate of the detector performances.

The test beam simulation includes:

- the exact geometry of the setup, with the same MAPMT configuration files used to reconstruct the experimental data;
- detailed description of the aerogel characteristics;
- full digitalization of the MAPMTs response;
- hadron tracks taken from the experimental data;

The optical properties of the aerogel are defined through a number of empirical parameters describing not only the propagation of the light inside the medium (as for example the scattering lenght or the dispersion), but also the surface effects. As an example, in Fig. 25 we show, for an aerogel sample with $n = 1.05$, the parametrization of the refractive index as a function of the wavelenght λ before (black curve) and after (red curve) the tuning to the experimental results of the test beam (red stars). The residual discrepancies at higher wavelenghts are due to the functional form implemented in **GEANT4**, however they are not particularly relevant because of the decrease of the MAPMT quantum efficiency in this spectral region [4].

The digitalization of the MAPMT response has been done by implementing the pixel structure of the H8500 tubes, including the dead spaces between the pixels and the global efficiency measured in the laser tests. Based on these tests, for each MAPMT hit, a 4% cross talk probability has been applied, i.e. 4% of the hit are shifted from the pixel that actually

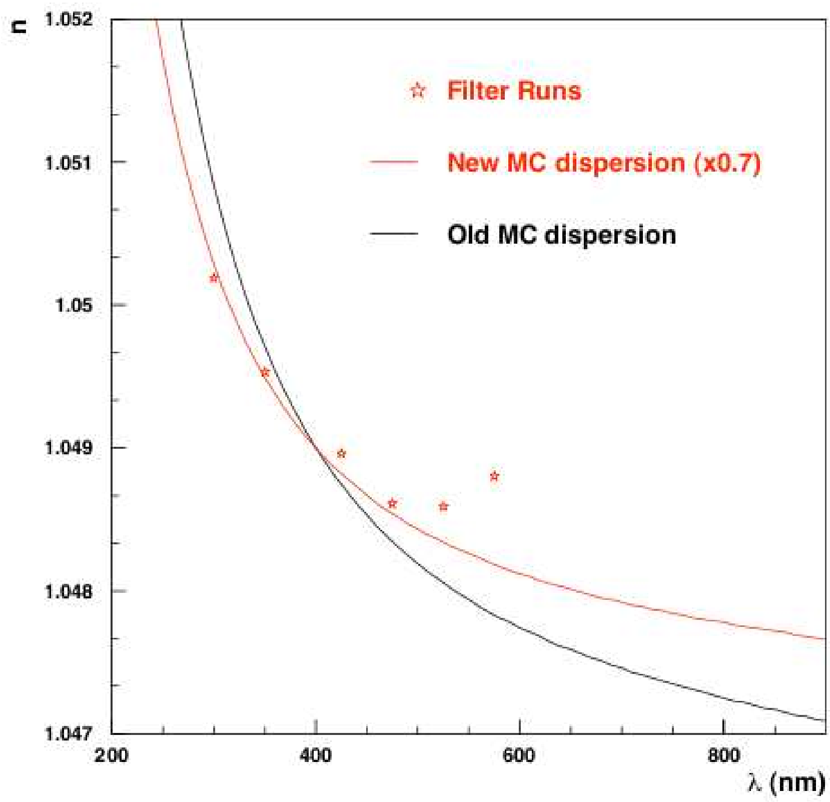

Figure 25: Dispersion curve for aerogel with $n = 1.05$ before (black curve) and after (red curve) the tuning to the experimental results of the test beam (red stars).

fired to one of the neighbours. Finally, at each event random dark counts with a probability of 10^{-4}, as measured in the test beam, has been added to the list of real hits.

We take as benchmark for the comparison with simulation the data taken with $n = 1.05$ and $t = 2$ cm (direct light) and $t = 6$ cm (reflected light). The quality of the agreement between data and simulation is shown in Fig. 26, where, for each of the 28 MAPMTs, the residual distributions from data (red histograms) and Monte Carlo (black histograms) are compared.

In Fig. 27, we show comparison of the photon yield and ring radius resolution between data and Monte Carlo. For the direct light data, the photon yields are very similar (about 13 p.e. per event) as well as the radii, for which we obtained $\sigma_R = 1.80$ mm in the experimental data and $\sigma_R = 1.87$ mm in the Monte Carlo simulation. Sligthly larger differences are found for the reflected light.

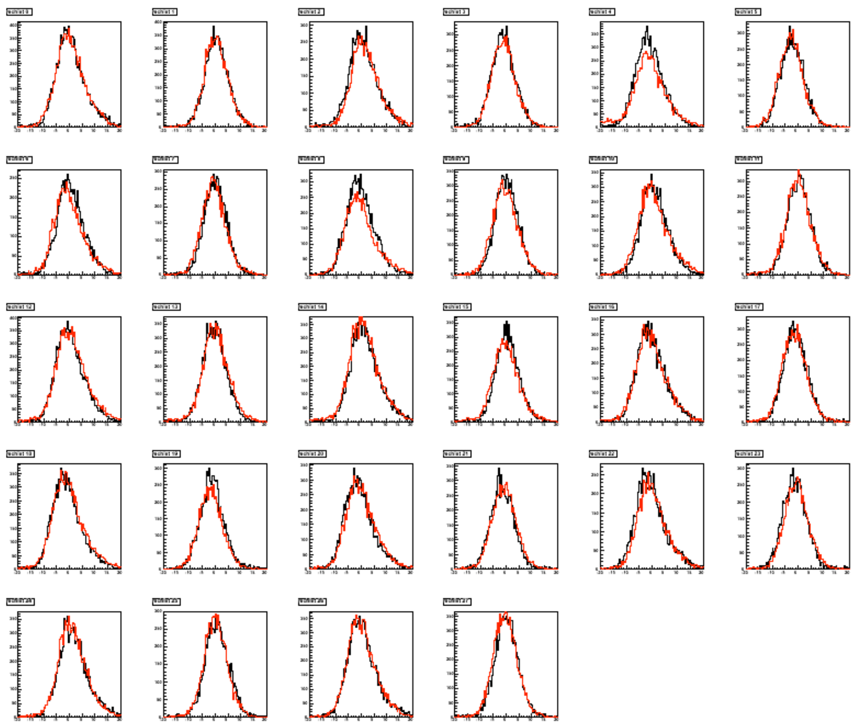

Figure 26: Residuals from experimental data (red histograms) and Monte Carlo simulation (black histogram) compared for each of the 28 MAPMTs. Measurements in the direct light configuration with aerogel with $n = 1.05$ and $t = 2$ cm.

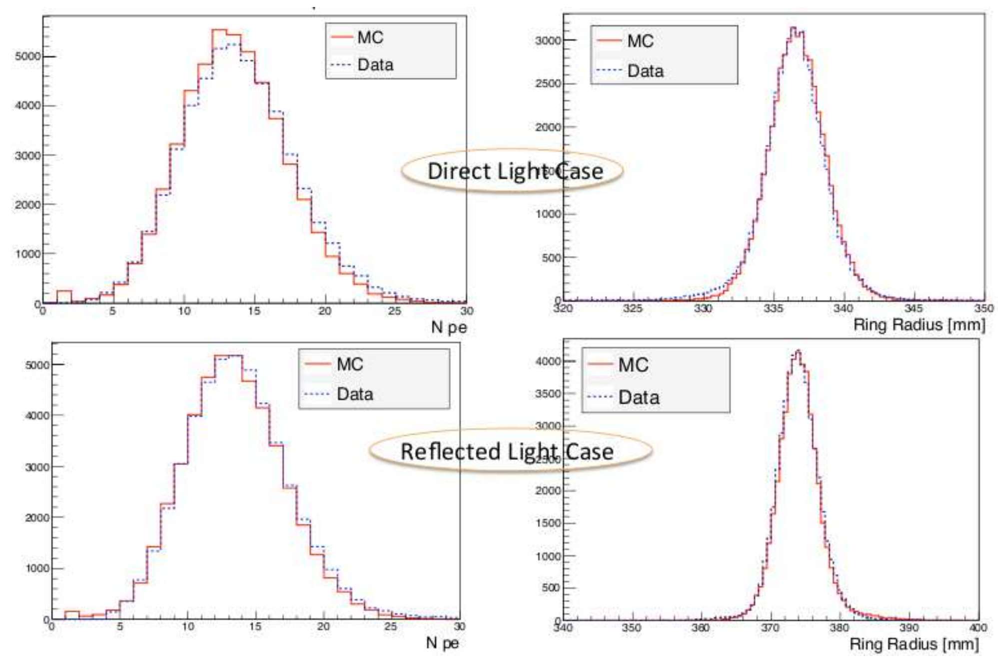

Figure 27: Photon yield (left plots) and ring radius resolution (right plots) for Monte Carlo and data: first row for direct light, second row for reflected light.

12 Summary from the test and possible improvements

For the direct light configuration, the pion/kaon separations measured with the prototype are reported in Tab. 2. The results match the requirements up to momenta of 7 GeV/c, while they are below the requirements at $P = 8$ GeV/c, though still above $n_\sigma = 3$. On the other hands, the measurements have also indicated the improvements that can be reached in the final detector.

In the prototype, we used 14 H8500 with normal glass and 14 with UV-enhanced glass. The latter ones provide on average one photoelectron more, but they also have a worse resolution, see Tab. 4. The single photon resolution measured with normal glass MAPMTs is in fact about 30% better than for UV-enhanced MAPMTs and about 15% better than the one measured with all the 28 MAPMTs. Thus we expect a corresponding improvement in the pion/kaon separation using only those normal glass MAPMTs.

Another improvement is the better ring coverage (close to the limit given by the H8500 packing fraction of 89%) that we will have in the final RICH. In the prototype, the coverage was worse by an additional factor of $15 - 25\%$ and, if we apply a cut $N_{pe} > 7$, we gain about 7% in resolution with a loss of pions of only 10%. Therefore, in the CLAS12 RICH we may reject the events with smaller number of Cherenkov hits, improving the resolution but without decreasing too much the efficiency.

The biggest contributions to the Cherenkov ring resolution come from the aerogel. By looking at the time evolution of the aerogel production shown in Fig. [3], further improvements may also be foreseen.

For the reflected light case, the test beam data give a pion/kaon separation at 6 GeV/c of about $n_\sigma = 2.6$. This value is below the requirements, however the prototype geometry was different from the one of the CLAS12 RICH, thus, dedicated simulations should be performed to estimate the expected performances of the RICH.

Nevertheless, in the prototype geometry the reflected light case will also benefit from the mentioned improvements, and in some case the expected effects would be even bigger. In fact, the fraction of ring covered by the MAPMTs was smaller than from the direct light data, thus the expected increase in the number of photoelectrons would be at least 30%. Another 15% resolution improvement would come from the use of normal glass window MAPMTs only. Further, the longer photon path length will help in the separation of the Cherenkov pion and kaon rings. Finally, any improvement in the aerogel quality would not only increase the number of produced photons, but also would reduce the yield depletion due to the double passage.

References

[1] CLAS12, FT[20]

[2] Aerogel Technical note, Table 1

[3] Aerogel Technical note, Figure 10

[4] MAPMT Technical note, Figure 1

[5] Aerogel Technical note, Equation 5

[6] Aerogel Technical note, Figure 4

[7] http://omega.in2p3.fr/index.php?option=com_content&view=article&id=99&Itemid=237